Stem Cells Translational Medicine, 2022, **11**, 715–726
https://doi.org/10.1093/stcltm/szac027
Advance access publication 28 May 2022
Brief Report

Partial Tendon Injury at the Tendon-to-Bone Enthesis Activates Skeletal Stem Cells

Ashley L. Titan[1,2,‡], Michael Davitt[1,‡], Deshka Foster[1,2], Ankit Salhotra[1], Siddharth Menon[1], Kellen Chen[1], Evan Fahy[1], Michael Lopez[1], R. Ellen Jones [1], Ioana Baiu[2], Austin Burcham[1], Michael Januszyk[1], Geoffrey Gurtner[1,2], Paige Fox[1], Charles Chan[1], Natalina Quarto[1,2], Michael T. Longaker[1,2,3,*]

[1]Hagey Laboratory for Pediatric Regenerative Medicine, Department of Surgery, Division of Plastic and Reconstructive Surgery, Stanford University School of Medicine, Stanford, CA, USA
[2]Department of Surgery, Stanford University School of Medicine, Stanford, CA, USA
[3]Institute of Stem Cell Biology and Regenerative Medicine, Stanford, CA, USA

*Corresponding author: Michael T. Longaker, M.D., M.B.A. D.Sc. (hon), FACS, 257 Campus Drive, MC 5148 Stanford, CA 94305-5148, USA. Tel: +1 650 736 1707; Fax: +1 650 736 1705; Email: longaker@stanford.edu
‡Contributed equally.

Abstract

The tendon enthesis plays a critical role in facilitating movement and reducing stress within joints. Partial enthesis injuries heal in a mechanically inferior manner and never achieve healthy tissue function. The cells responsible for tendon-to-bone healing remain incompletely characterized and their origin is unknown. Here, we evaluated the putative role of mouse skeletal stem cells (mSSCs) in the enthesis after partial-injury. We found that mSSCs were present at elevated levels within the enthesis following injury and that these cells downregulated TGFβ signaling pathway elements at both the RNA and protein levels. Exogenous application of TGFβ post-injury led to a reduced mSSC response and impaired healing, whereas treatment with a TGFβ inhibitor (SB43154) resulted in a more robust mSSC response. Collectively, these data suggest that mSSCs may augment tendon-to-bone healing by dampening the effects of TGFβ signaling within the mSSC niche.

Key words: skeletal stem cell; enthesis; tendon-to-bone interface; Achilles injury

Graphical Abstract

mSSCs Downregulate TGFB Signaling in order to Permit Their Expansion and Contribution to Tendon Enthesis Regeneration

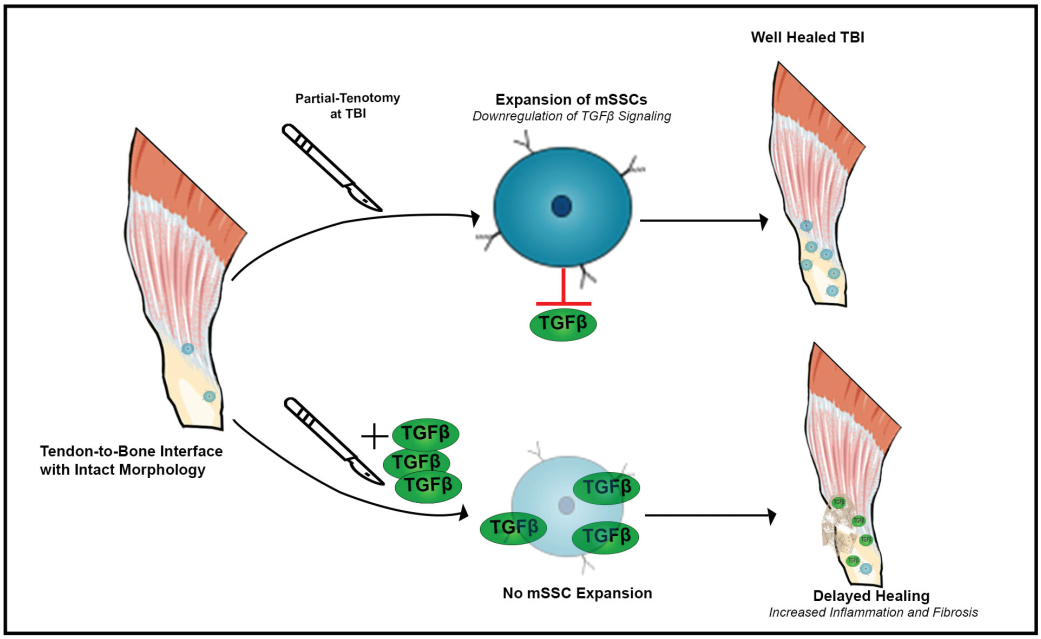

Received: 28 October 2021; Accepted: 9 March 2022.

Significance Statement

Tendon regeneration is of critical importance in achieving full recovery among the millions of patients with mechanical musculoskeletal injuries. Once injured, the tendon enthesis can never fully recover to its pre-injury function. The cells involved in the healing process are not well characterized and their origin is unknown. We found that mouse skeletal stem cells (mSSCs) play a fundamental role in the tendon enthesis by augmenting healing and potentially suppressing inhibitors such as TGFβ, which otherwise preclude a full tendon recovery.

Introduction

The tendon enthesis or tendon-to-bone interface (TBI) is a complex structure that plays a critical role in facilitating movement and reducing stress within joints.[1] This fibrocartilaginous enthesis is composed of diverse cell types to permit the transfer of mechanical forces between bone and tendon—2 tissues with dramatically different material and cellular properties.[1-4] The enthesis is classically described as being composed of 4 zones, representing a gradient of mechanical and cellular properties: the tendon (containing organized collagen fibrils and tenocytes with Young's modulus of 0.2 GPa), uncalcified fibrocartilage, calcified fibrocartilage, and bone (containing organized lamellar structure with Young's modulus of 20 GPa).[1-9]

Following enthesis-injury, the enthesis is unable to fully regenerate and never regain its uninjured morphological appearance, which increases the risk of recurrent injury.[2,4,10] There is extensive histological data available characterizing tendon healing.[11] However, the underlying cellular and molecular mechanisms contributing to tendon-to-bone pathogenesis and healing remain largely unknown.[12]

Our group has previously isolated and identified mouse skeletal stem cells (mSSCs) from a variety of skeletal tissues including long bones,[13-15] mandibles,[16,17] and cranial sutures.[18] They are defined by their ability to self-renew and their multilineage contribution to bone, cartilage, and stroma, but not fat.[13,15-20] Its downstream progenitor is bone, cartilage, and stromal progenitors (BCSPs).[13,16,20-22] They have both been shown to be key facilitators in bone development, maintenance of homeostasis, and response to fracture healing.[13,15-20] In this study, we evaluated whether mSSCs participated in the physiologic response to tendon injury at the enthesis and whether modulation of their activity may improve healing. This study, to our knowledge, represents the first characterization of the mSSC response to enthesis injury and may have broad implications for similar musculoskeletal pathology specifically partial TBI injuries that go untreated (eg, partial rotator cuff tears undergoing physical therapy in humans).

Methods

Subject Details

We purchased 9-week-old Black 6 (C57BL/6J, stock number: 000664) mice from Jackson Laboratories. Rainbow mice (ROSA26VT2/GK3) were provided as a gift from the Weissman Laboratory, Stanford University School of Medicine. Mice were housed at the Stanford University Comparative Medicine Pavilion. The facilities provided light and temperature-regulated housing for all animals. A minimum sample size of 3 replicates per group was used for all experiments (exact numbers for specific experiments are provided in the figure legends). All experiments were carried out in accordance with the Stanford IACUC standards of care and approved by the institutional ethics committee, Administrative Panel on Laboratory Animal Care, (protocol reference: 9999).

Partial Tenotomy Mouse Model

Mice were anesthetized with inhaled isoflurane (Henry Schein Animal Health) at a concentration of 1-2% in oxygen at 3 L/minute on top of a heating pad to ensure the mice were kept warm throughout the procedure. To prevent corneal desiccation ophthalmic ointment (Puralube petrolatum, Dechra Veterinary Products) was applied to the cornea. The mice were placed in the prone position on a clean operating surface. For the partial tendon injury at the tendon-to-bone enthesis, the left posterior foot, ankle, and lower leg were sterilized with 3 applications of betadine followed by 70% ethanol. Using the aseptic technique, an incision was made over the calcaneus and extended 1 cm proximally. The distal Achilles was dissected free from the surrounding tissues and then just above the tendon-to-bone interface a partial injury (~50%) of the tendon was transected using micro-scissors (Fine Science Tools, UK). The skin was closed using a 6-0 nylon suture (Ethilon). On the contralateral limb, a sham skin incision procedure was performed and was closed using a 6-0 nylon suture (Ethilon). During the procedure, the respiratory rates of the animals were monitored and the isoflurane was titrated accordingly. All mice were monitored daily until sutures were removed. For the mid-substance injury, the same sterile technique was used as well as the same incision. The Achilles was dissected free from the surrounding tissues and then in the mid aspect of the tendon, a partial injury (~50%) was created using micro-scissors (Fine Science Tools, UK). The skin was closed in a similar fashion as the previous procedure.

Liposomal Tamoxifen Induction for Rainbow Reporter System

Activated tamoxifen liposomes (LiTMX) were prepared as described by Ransom et al.[23] Briefly, a 90:10 mol:mol mixture of 1,2-dimyristoyl-*sn*-glycero-3-phosphocholine and cholesterol (Avanti Polar Lipids) was desiccated under 5 kPa stream of nitrogen gas for 5 min. This was followed by vacuum desiccation at 25 °C for 3 h, sonication in 1× PBS for 15 s, and then reconstitution by extrusion using a 100-nm pore-diameter polycarbonate membrane (Sigma-Aldrich) at 32 °C. Using NanoBrook Omni dynamic light scattering (DLS) instrument (Brookhaven) the liposome size was confirmed. Liposomal vesicles were then incubated with 4-hydroxytamoxifen (Sigma–Aldrich) under nitrogen gas at 25 °C for 6 h. LiTMX was applied locally to injury sites or areas of interest (tendon-to-bone interface) for induction of Cre Recombinase at the time of surgery for Rainbow mice.

Exogenous Delivery of TGFβ

Two micrograms of exogenous carrier-free TGFβ-1 (10 μL, Biolegend, Cat# 763102) were delivered locally (adjacent to the tendon-to-bone interface) at the time of surgery before

skin closure. The procedure was conducted as described above. Additional doses of 2 µg were given every 3 days via a Hamilton syringe for fluorescence-activated cell sorting (FACS) and every other day for gross and histological analysis (700 Series, Hamilton). Achilles entheses were harvested at 3 and 7 days after surgery for FACS sorting as described below. Saline administration was used for control.

Exogenous Delivery of SB431542

A total of 10 µM SB431542 formulated in DMSO (10 µL, selleckchem, Cat# S1067) was delivered locally (adjacent to the tendon-to-bone interface) at the time of surgery after the skin closure of mice. The procedure was conducted as described above. Additional doses of 10 µM were given every other day at the injury site via a Hamilton syringe for FACS and every other day for gross and histological analysis (700 Series, Hamilton). Achilles TBIs were harvested at 3 and 7 days after surgery for FACS sorting as described below. Saline administration was used for control.

Tissue Processing and Histology

Mouse injured and control tissues were fixed in 4% paraformaldehyde (Electron Microscopy Sciences) for 20 h at 4 °C. The specimens were decalcified in 19% EDTA in PBS at 4 °C for 4 weeks with a change of EDTA every 48 h. Specimens were then placed in 30% sucrose (Sigma–Aldrich) until saturation at 4 °C following fixation, followed by OCT until saturation at 4 °C, embedded in OCT, and sectioned at 8 µm on Superfrost Plus microscope slides (FisherScientific). Representative tissue specimens were stained with a modified pentachrome using the protocol routinely used in our laboratory.[16]

Immunohistochemistry

Immunohistochemistry of TBI cryosections was performed using vectastain elite ABC Kit (Vector Laboratories) according to the manufacturer's instructions. In brief, samples previously cut in 8 µm sections on Superfrost Plus microscope slides (Fisher Scientific) were rehydrated and endogenous peroxidases were quenched using 3% H_2O_2 for 10 min. Sections were then treated with heated Tri-base (Sigma–Aldrich) for 15 min, permeabilized with 0.5% Triton-X-100. 1X Power Block (BioGeneX) in combination with avidin/biotin blocking kit (Vector Laboratories) was applied for 1 h at room temperature. Sections were then incubated with the primary antibody (SP7, Abcam, ab22552, dilution 1:100) at 4 °C overnight. Subsequently, the respective secondary antibody (prediluted RTU Biotinylated Goat Anti-Rabbit IgG Antibody, Vector Laboratories, BP-9100-50) was incubated on the specimen for 90 min. The specimens are rinsed and then incubated for 1 minute using DAB (BD Sciences, Cat# 550880, dilution 1:500). Specimens were next washed with PBS, cover-slipped, and imaged with a Leica DMI6000B inverted microscope system.

Cell Culture and Immunofluorescence

FACS-isolated mSSC were plated in chambered slides coated with 0.1% gelatin and cultured in MEM alpha medium with 10% fetal bovine growth serum (FBS), 1% penicillin-streptomycin. After at least 48 h cells were washed twice with phosphate-buffered saline (PBS) and fixed with 50% acetone-50% methanol for 20 min at 4 °C, followed by washing with PBS–0.1%Triton-100 twice. Then, cells were incubated in a blocking solution with 1% horse serum in PBS–0.05% Tween-20 for 1 h at RT followed by incubation with a primary rabbit Phospho-SMAD2 (Ser465, Ser467) Antibody (Invitrogen, Cat# 701582, dilution 1:250) for 3 h at room temperature. After, cells were washed 3 times with PBS/0.1% Tween-20 and incubated in the blocking solution for 1 h at room temperature followed by incubation with FITC-conjugated Goat Anti-Rabbit secondary antibody (Abcam, Cat# ab6717, dilution 1:500) for 45 min at room temperature. Nuclear counterstaining was performed using Vectashield H-1200 mounting medium with DAPI (Vector Laboratories).

Confocal Imaging and Analysis

The cryopreserved 8-µm sections on Superfrost Plus microscope slides (Fisher Scientific) as well as the chambered cell culture slides were imaged using laser scanning confocal microscopy via the Leica WLL TCS SP8 Confocal Laser Scanning Microscope (Leica Microsystems) located in the Cell Sciences Imaging Facility (Stanford University, Stanford, CA). The 10× objectives were used (10× HC PL APO, air, N.A. 0.40). Image analysis was performed using Fiji software (ImageJ, NIH). Photoshop was utilized for image intensity analysis using the histogram tool.

Biomechanical Testing

Within 2 h of sacrifice, the Achilles TBI underwent mechanical testing. During the dissection and mechanical testing, samples were kept moist by regular spraying with 10% PBS. Dimensional measurements of the tendon-to-bone interface were performed using a digital micrometer with fine tips and a resolution of 0.01 mm under microscope dissection by one user. Custom grips were used to compressively grip proximally at the Achilles tendon and distally at the calcaneus. The angle of pull was 180°. As per Beason et al, tendons were preloaded to 0.02 N to remove slack and the length of the tendon was measured.[24] The length of the tendon was designated as the distance between the grip ends (ie, the distance of the entire tendon subjected to the displacement). To provide a consistent strain history, the tendons were exposed to 10 cycles of preconditioning from 0.02 N to 0.05 N at a rate of 0.1%/s. After a 300 s hold, tendons were then loaded to 5% strain at a rate of 25%/s and then held for stress relaxation over 600 s. Finally, tendons were unloaded back to 0% strain and then immediately subjected to an extension test to failure at a rate of 2%/s.[24,25] Young's modulus was calculated by taking a least-squares regression of the slope at the individual linear portion of the extensional test. Yield force, stress, and strain were taken at the point of the curve which exited linear deformation and entered plastic deformation. Stress was calculated by dividing the force by the cross-sectional area. The strain was measured by dividing the displacement over the original length of the tendon. Stress, strain, and modulus calculations were made using MATLAB (MathWorks).

Sample Preparation and FACS Isolation

The detailed steps listed in Gulati et al[14] were followed for sample preparations and FACS isolation mSSCs. Specimens, including either the TBI or mid-tendon, were dissected and then were gently minced with a dissecting scissor on ice. They were then serially digested in collagenase digestion buffer at 37 °C for 30 minutes under constant agitation in an orbital

shaker at 275 rpm at 37 °C. Digest consisted of serum-free Medium 199/EBS (HyClone) supplemented with 1.6 mg/mL Collagenase Type II (Sigma-Aldrich, Cat# 6885) 2 mg/mL Dispase II (Roche Diagnostics), 1% bovine serum albumin (Sigma-Aldrich), 1% pluronic F-68 (Gibco-Life Technologies), 2% HEPES buffer (Gibco-Life Technologies, Grand Island, NY, USA), 0.4% 2.5 M $CaCl_2$ (Sigma-Aldrich), 100 units/mL deoxyribonuclease I (Worthington Biochemistry). Dissociated cells were filtered through a 70 µm mesh filter, pelleted at 300*g* at 4 °C, resuspended in FACS buffer which was composed of PBS (Gibco-Life Technologies), 2% fetal bovine serum (Gibco-Life Technologies), 1% penicillin-streptomycin (Gibco-Life Technologies), 1% pluronic F-68 (Gibco-Life Technologies). The digestions were pooled together and total dissociated cells were pelleted at 300*g* at 4 °C, resuspended in FACS buffer.

Cells were stained with fluorochrome-conjugated antibodies CD45 (Biolegend, Cat# 103110), Ter119 (ThermoFisher, Cart# 15-5921-81, dilution 1:200), CD202/TIE2 (eScience, Cat# 14-5987-81, dilution 1:20), Thy1.1 (ThermoFisher Cat# 47-0900-82, dilution 1:100), Thy 1.2 (ThermoFisher Cat# 47-0902-82, dilution 1:100), CD105/6C3 (ThermoFisher, Cat# 13-1051-85, dilution 1:100), CD51 (BD Sciences, Cat# 551187, dilution 1:50), CD 200 (BD Sciences, Cat# 745255, dilution 1:50), goat anti-rat IgG secondary antibody (ThermoFisher, Cat# Q-11601MP, dilution 1:50), and Alexa Fluor 680 Fluorophore Antibody (ThermoFisher, Cat# A20188, dilution 1:20). Stained cells were pelleted at 300*g* at 4°, resuspended in 300 µL of FACS buffer 70 µm filter for flow cytometry. For information regarding antibodies used for FACS isolation of skeletal stem/progenitor cells refer to Supplementary Table S1.

Flow cytometry was performed on the FACS Aria II in the Lorey Lokey Stem Cell Institute Shared FACS Facility. First, CD45+ and dead cells (Pi+) were fractionated out and the remaining population (P3) was fractioned based upon previously described antigens by Chan et al[13] and Gulati et al[14] The mSSC profile was CD45–, Ter119–, Tie2–, Thy1.1–, Thy1.2–, 6C3–, CD105–, CD51+, and CD200+. The mBCSP profile was CD45–, Ter119–, Tie2–, Thy1.1–, Thy1.2–, 6C3–, CD51+, and CD105+. The sequential FACS gating strategy is shown in Supplementary Fig. S2. Cells were sorted directly into TRIzol Reagent (Ambion-Life Technologies) for RNA isolation and extraction or alpha-MEM supplemented with 20% fetal bovine serum, and 1% penicillin-streptomycin (Gibco-Life Technologies) for cell culture and differentiation assays.

Bulk mRNA Sequencing

mSSCs, freshly isolated from 3 groups of 5 pooled injured or control TBIs of C57BL/6J mice were sorted directly into TRIzol Reagent (Ambion-Life Technologies). All cells collected were used for RNA extraction. The average number of cells collected for each pooled group was 2140 ± 3487 cells. RNA extraction was performed using Qiagen miRNeasy kit with one column DNAse treatment per the manufacturer's recommendations. To generate cDNA from 1 ng total RNA, the Clontech Smarter Ultra Low Input RNA kit (Takara Bio) was used per the manufacturer's recommendations. Amplified cDNA was purified using SPRI Ampure Beads (Beckman Coulter) and the quality and quantity were measured using a high sensitivity DNA chip on the Agilent 2100 Bioanalyzer (Agilent Technologies). The cDNA was enzymatically fragmented to an average of 300 base pairs and libraries were generated with the Nextra-Xt kit (Illumina). The samples were uniquely barcoded, pooled, and sequenced on a single lane of the HiSeq (Illumina). A total of 263 million paired-end reads were obtained, with a minimum threshold of 37.5 million reads per sample.

Bulk mRNA Sequencing Data Analysis

A total of 6 samples (3 injured and 3 control samples containing pooled 5 specimens each) were profiled by bulk RNA sequencing at post-injury day 7 as described above. Raw FASTQ reads were aligned to GENCODE vM20 reference transcripts (GRCm38.p6) for a mouse with Salmon v0.12.0 using the -seqBias, -gcBias, -posBias, -useVBOpt, -rangeFactorizationBins 4, and -validateMappings flags and otherwise default parameters for single-end mapping. Count normalization and differential gene expression analysis were performed using the DESeq2 v1.22.2 package in R. Counts were size-factor normalized using the "DESeq" function and log_2-transformed. Pairwise differential gene expression analysis was performed using the lfcShrink function with "type = apeglm," which applies an adaptive *t* prior shrinkage estimator. Principal component analysis (PCA) was used to evaluate aggregate separation between injury and control (sham-surgery) transcriptomes. Gene enrichment analysis was performed on ranked lists of differentially expressed genes (n = 500 genes), ordered by adjusted *P*-value, using the enrichR toolkit against the KEGG, WikiPathways, and Gene Ontology databases.[26,27] Additional analysis was performed using subsets of these genes that were specifically upregulated (n = 247) and downregulated (n = 253).

RT-PCR Analysis for Genes Expression

To analyze the expression level of genes of interest, RNAs were isolated from cells using the Trizol (Ambion-Life Technologies, Carlsbad, CA) procedure according to the manufactures' instructions. Isolated RNAs were submitted to RT-PCR procedure as previously described.[28] Primer-sequences for *Col1a, PAI1,* and *Gapdh* genes, and annealing temperatures ions are reported in Supplementary Table S2.

Statistical Analysis

Statistical analyses were performed using the software GraphPad Prism v.6. Results are expressed as absolute numbers, percentages, or means ± SD. Data analysis was performed using an unpaired *t*-test assuming 2-tailed distribution or one-way analysis of variance (ANOVA) and post hoc Tukey correction were used to compare groups where relevant. Fisher's exact test was used for gene ontology analysis.[26,27] Statistical significance was assigned for $P \leq .05$.

Results

Mouse Achilles TBI Injury Model

The cellular mechanisms responsible for TBI healing after injury remain poorly characterized. We aimed to evaluate whether new tissue formation within the injury site involved tissue-resident skeletal stem cells. We used a mouse partial Achilles TBI tenotomy model known to alter the mechanical loading of the enthesis, resulting in impaired healing that never fully recapitulates normal morphology (Fig. 1A; Supplementary Fig. S1A). Using this model, we confirmed that the biomechanical properties of the TBI were significantly altered. The linear region of the stress–strain curve was significantly reduced at

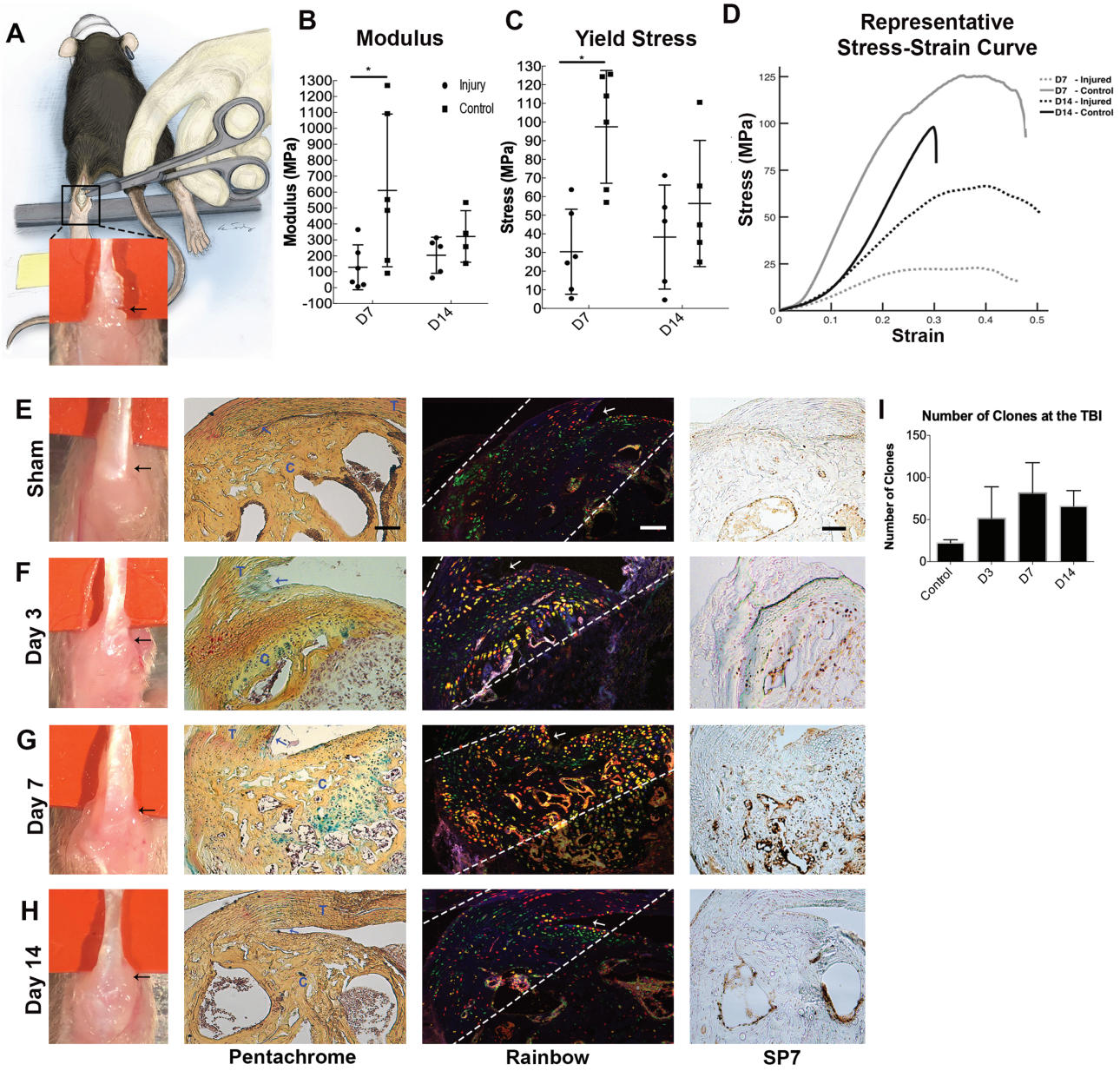

Figure 1. Tissue and cell clonality characterization of partial Achilles tenotomy model. (**A**) Illustration and gross imaging of partial Achilles tenotomy model. (**B**) Elastic modulus of the Achilles TBI is significantly decreased 7 days post-injury (n = 6 per group). (**C**) The linear region of the stress–strain curve of an injured Achilles TBI is significantly less than the sham control at 7 days (n = 6 per group). (**D**) Representative stress–strain curve (n = 6 per group). (**E-H**) Gross imaging, pentachrome staining, confocal micrographs, and SP7 immunohistochemistry of transverse TBI sections from ActincreERT2; RosaR26mice which were locally induced with activated tamoxifen liposomes using a published protocol at the time of surgery,[23] harvested at 3, 7, and 14 days post-surgery, clonal proliferation are visualized within the calcaneus at day 3, and by day 7 there was clonal proliferation within the calcaneus and along with the injury at the enthesis (noted by an arrow). (**I**) Quantification of the average number of clones at the injury site after injury (POD3-14, n = 3 per group). Representative samples calcaneus and tendon are labeled respectively as "C" and "T" an arrow marks the injury (n = 3 per group). Scale bars, 100 μm. Data and error bars are shown as mean ± SD. *P < .05, unpaired 2-tailed t-test.

post-injury day 7 (control 97.4 ± 30.2 MPa vs. post-injury day 7 30.4 ± 22.8 MPa; P = .005); the elastic modulus was also significantly reduced 7 days after injury (control 610.1 ± 479.2 MPa vs. post-injury day 7 128.2MPa ± 140.9 P = .02; Fig. 1B-1D; Supplementary Fig. S1B, S1C).

Polyclonal Expansion After Partial Achilles TBI-Injury

We began by assessing the extent of the clonal proliferation of local cells in Achilles TBI after injury. We created a partial Achilles TBI tenotomy to mimic tendon TBI injury in rainbow mice (*Actin*^{creERT2}; *Rosa*^{R26}), given that no existing genetic drivers are known to delineate mSSC clonal proliferation. These rainbow mice express a Cre-inducible fluorescent reporter under the ubiquitous Actin promoter following tamoxifen induction. After recombination, cells express one of 4 colors (eGFP, mCerulean, mCherry, and mOrange). The resulting progeny are marked with the same color as the parent cell.[29,30] To achieve tissue-specific rainbow induction, we applied liposomes at the region of interest immediately following injury.[23] Local administration of 4-hydroxytamoxifen liposomes instead of systemic tamoxifen injection was performed to ensure that

only tissue-resident cells would be labeled. This would avoid labeling any cells outside of the local environment.

Histologically, we observed both gradual TBI repair and bone remodeling of the calcaneus (Fig. 1E-1H, Supplementary Fig. S1D, S1E). On confocal microscopy, we observed an increased number of single-colored clones at the TBI after injury (Fig. 1E-1I). On immunohistochemistry, we noted increased expression of the SP7 protein, a known regulator of osteoblast differentiation and associated with bone formation, at post-injury day 7 compared to sham control[31-33] (Fig. 1E-1H). Taken together, these findings suggest that cells of skeletal origin proliferate clonally in response to TBI-injury.

mSSCs Are Present Within the TBI at Homeostasis and Proliferate in Response to Injury

Since we had previously observed that mSSCs are enriched in mouse skeletal tissues after injury,[13-18] we evaluated TBI cells using a similar strategy with FACS[13-18] (Fig. 2A, Supplementary Fig. S2). We collected tissues from sham control Achilles TBI and tendon mid-substance (mid-tendon). We identified the presence of mSSCs and their downstream bone-cartilage-stromal progenitors (mBCSPs) within both tissues and found a significantly larger representation of mSSCs and mBCSPs within the TBI compared to the mid-substance (Fig. 2B).

Subsequently, we sought to determine how mSSCs respond to TBI and/or mid-substance injury. We performed partial Achilles tenotomies at either site, utilizing the contralateral leg as a sham surgery control. This experiment uncovered a significant mSSCs expansion 7 days post-injury in response to TBI-injury, but not after mid-substance injury (Fig. 2C, 2D). Similarly, TBI injury elicited an expansion of mBCSPs, suggesting that both progenitor populations in this tissue are injury-responsive.

TBI-Injury-Specific mSSC Gene Regulation

To characterize gene expression changes associated with mSSC in response to injury, we FACS-isolated injured and sham control mSSCs for bulk RNA-seq analysis. Clear differences were observed between injury and control transcriptomes (Fig. 3A). Using enrichment analysis, we evaluated the top 500 genes with the greatest difference in expression between injury vs. sham mSSCs (Fig. 3B). Genes upregulated in injured mSSCs suggest these cells were locally activated. Specifically, *Panx3*, associated with cellular activation of differentiation pathways including osteogenesis and chondrogenesis,[34-36] was significantly upregulated in injured mSSCs. Additional pathways upregulated in injured mSSCs suggesting that the mSSCs are actively playing a role in TBI healing were the Indian hedgehog (*Ihh*) pathway linked to TBI fibrocartilage development and mineralization,[37-39] glycosaminoglycan biosynthesis (data not shown, see the Gene Expression Omnibus for bulk RNA data), known to be an important part of the extracellular matrix in managing TBI compressive forces,[40] and in cell cycling suggesting that mSSCs are being activated to replicate and possibly differentiate (Fig. 3C, 3D; Supplementary Fig. S3A).

Interestingly, we found an overall downregulation of TGFβ pathway-components, indicated by downregulation of *Tgfβ1*, *Tgfβr2, Smad3*, and upregulation of *Fbn1*, known to control the bioavailability of TGFβ[41] (Fig. 3C). Gene set enrichment analysis also highlighted the downregulation of TGFβ receptor binding pathways in injured mSSCs (Fig. 3D). BMP and FGF signaling have been shown to facilitate differentiation into enthesis components[42-44]; however, there were no significant changes in the expression of genes associated with these 2 signaling pathways in mSSCs following injury, suggesting that these mechanisms may not play a significant role in mSSC activation during TBI healing.

To confirm our RNASeq findings that TGFβ signaling is downregulated in injured mSSCs, we performed immunofluorescence of injured and control mSCCs investigating the expression of pSMAD2. SMAD is a major receptor-activated downstream effector of TGFβ signaling..[45] There was a decrease in the intensity of expression and in the number of cells that had positive pSMAD2 nuclear staining thus, suggesting that there may be the downregulation of TGFβ signaling in mSSCs after injury (Fig. 3E, 3F). Further confirmation of the differential activation of TGFβ signaling between uninjured and injured mSSCs was obtained from the PCR expression analysis of 2 specific targets of activated TGFβ signaling, *Col1a*, and *PaI1*.[46,47] These 2 genes were found to be upregulated in sham control mSSCs as compared to injured mSSC (Fig. 3G). The above findings strongly indicate that there is a difference in TGFβ signaling between injured and uninjured mSSCs.

Artificially Elevated Levels of Active TGFβ-1 After Injury Reduce the mSSC Response and Worsen TBI Healing

Over-activation of TGFβ signaling in the bone after partial mouse Achilles tendon injury is known to contribute to enthesopathy, whereas inhibition of TGFβ via an exogenous TGFβ neutralizing antibody improves tendon-to-bone healing.[12] The response to TGFβ signaling relies on precise spatial and temporal activation; if altered, as seen in TBI healing, the alignment of enthesis fibrocartilage cells and proteoglycan synthesis is disturbed.[48,49] Given the downregulation of gene expression of several components of the TGFβ signaling pathway within the mSSC niche after partial-injury, we sought to investigate the effects of modulating TGFβ signaling on the mSSC response. We applied exogenous TGFβ-1 to TBI sites and found that TGFβ-1 treatment led to a significant inhibition of the normal mSSC and mBCSP expansion at 7 days post-injury (Fig. 4A). Histologically, there was increased tissue disorganization and enthesopathy-like morphology seen in TGFβ1 treated TBIs (Supplementary Fig. S4). Grossly, we saw delays in healing with a profound inflammatory and fibrotic response in injuries treated with exogenous TGFβ-1 (Fig. 4B). These results further support prior research that the presence of excess TGFβ after TBI injury results in poor TBI healing and the possible inhibition of mSSC expansion (Fig. 4C).

We then examined whether functional modulation of TGFβ may affect TBI healing and the mSSC response using the small-molecule inhibitor SB431542. SB431542 is a selective inhibitor of the TGFβ superfamily type I activin receptor-like kinase receptors, which have been explored in a variety of fibrotic pathologies.[50,51] It has been previously shown in a mouse model of massive rotator cuff tear results in decreased fibrosis, fatty infiltration, and muscle weight loss after injury.[50] When this inhibitor was applied at the location of the injury, we found that there was a significant expansion of mSSCs and mBCSPs in both wild-type mice (Fig. 4A). Grossly, in mice treated with the inhibitor we saw a dramatic decrease in both fibrotic and inflammatory responses, compared to mice treated with exogenous TGFβ (Fig. 4B). Unexpectedly, the administration of SB431542 also improved the biomechanical

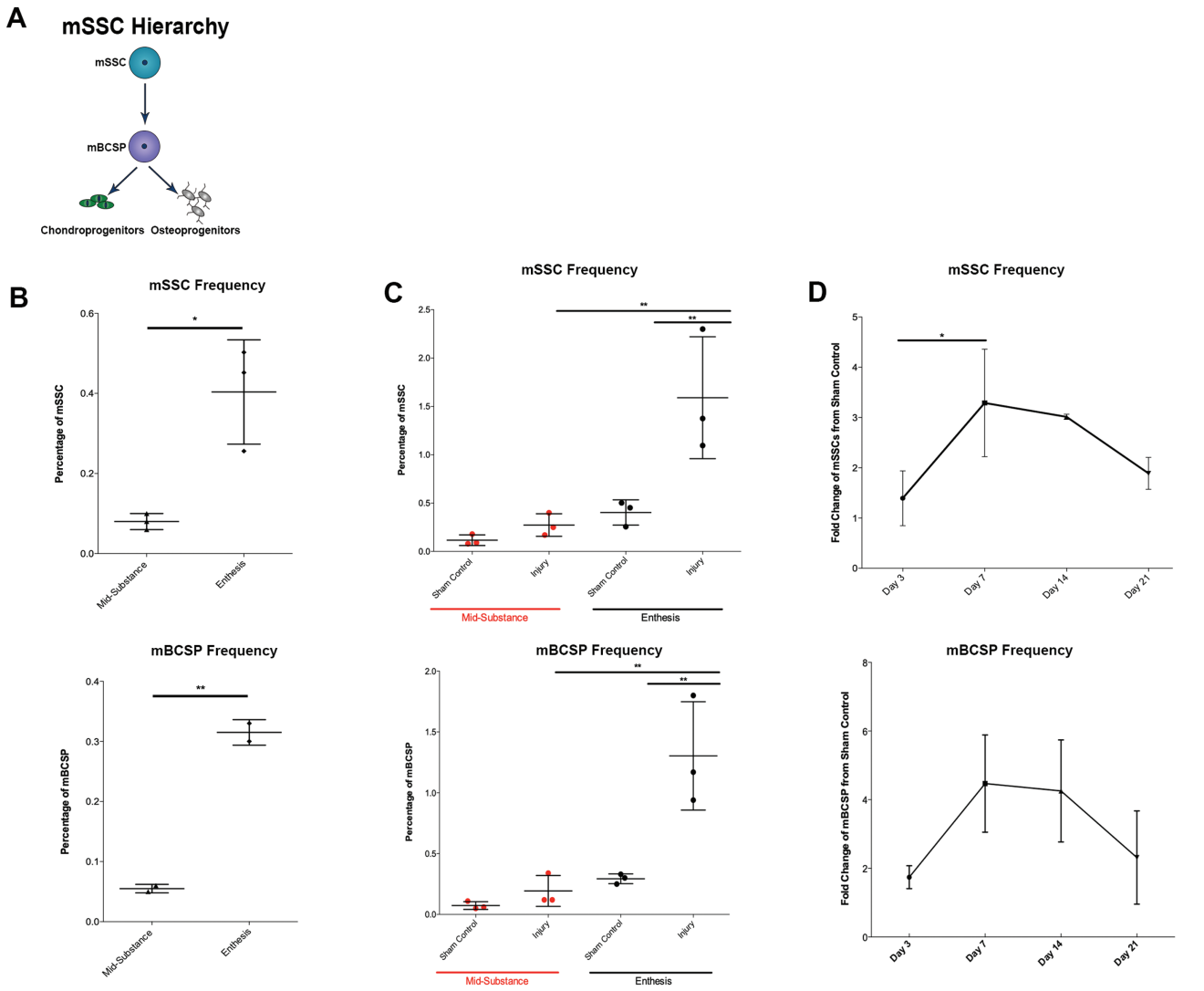

Figure 2. Identification of mSSCs in the Achilles tendon. (**A**) Illustration of the mSSC hierarchy. (**B**) Quantification of cellular frequency of FACS isolated mSSCs showing significantly more mSSCs within a sham control enthesis compared to the sham control mid-substance (n = 5 pooled, with 3 replicates). (**C**) Quantification of cellular frequency of FACS isolated mSSCs and mBCSPs demonstrating a significant increase within enthesis post-injury, but not within the mid-substance (n = 5 pooled, with 3 replicates). (**D**) Quantification of mSSC and mBCSP cellular frequency within enthesis post-injury with the maximum fold increase in mSSC occurring at post-injury day 7 (n = 5 pooled, with 3 replicates). Scale bars, 100 μm. Data and error bars are shown as mean ± SD. *P < .05, **P < .01, unpaired 2-tailed t-test.

properties of the injured TBI compared to treatment with PBS, as a control as well as treatment with TGFβ (Fig. 4D, 4E; Supplementary Fig. S4B). This outcome may reflect that TGFβ has a negative impact on the tissues within the TBI.

Discussion

The inability of the enthesis to fully recapitulate its mechanical and morphological properties after a partial injury leaves it at high risk for future rupture. In this study, we identified mSSC as a cellular component of the TBI at homeostasis and observed their activation, in concert with their likely downregulation of TGFβ signaling, following TBI-injury. Furthermore, we found that mSSC representation was dramatically decreased in mice treated with exogenous TGFβ-1 immediately following injury.

TGFβ plays an important role in cartilage and bone homeostasis, the development of tendons and bony eminences/interfaces, and the regulation of embryonic progenitor specification.[43,52,53] It is secreted in an inactive, latent form and deposited in the extracellular matrix. Several physiological processes result in the conversion of inactive TGFβ protein to its active form. However, excessive active TGFβ uncouples bone remodeling and contributes to the pathogenesis of osteopenia, Camurati-Engelmann disease, and other skeletal diseases.[12,54,55] High concentrations of active TGFβ-1 in the TBI have been shown to cause enthesopathy-like-states and the use of TGFβ-1 inhibitors after tendon injury has been shown to reduce fibrosis.[12,50,56,57] Our transcriptomic profiling identified a downregulation in the expression of several TGFβ signaling components in mSSCs isolated from injured-TBI in wild-type mice. In addition, our transcriptomic data suggests TGFβ signaling downregulation is seen within mSSC the population present after TBI injury.

Previous studies have found that TGF-β1 localizes to forming scar tissue after TBI injury[57] and increases the formation of fibrous tissues at the healing site by increasing collagen accumulation without the expansion of tenogenic

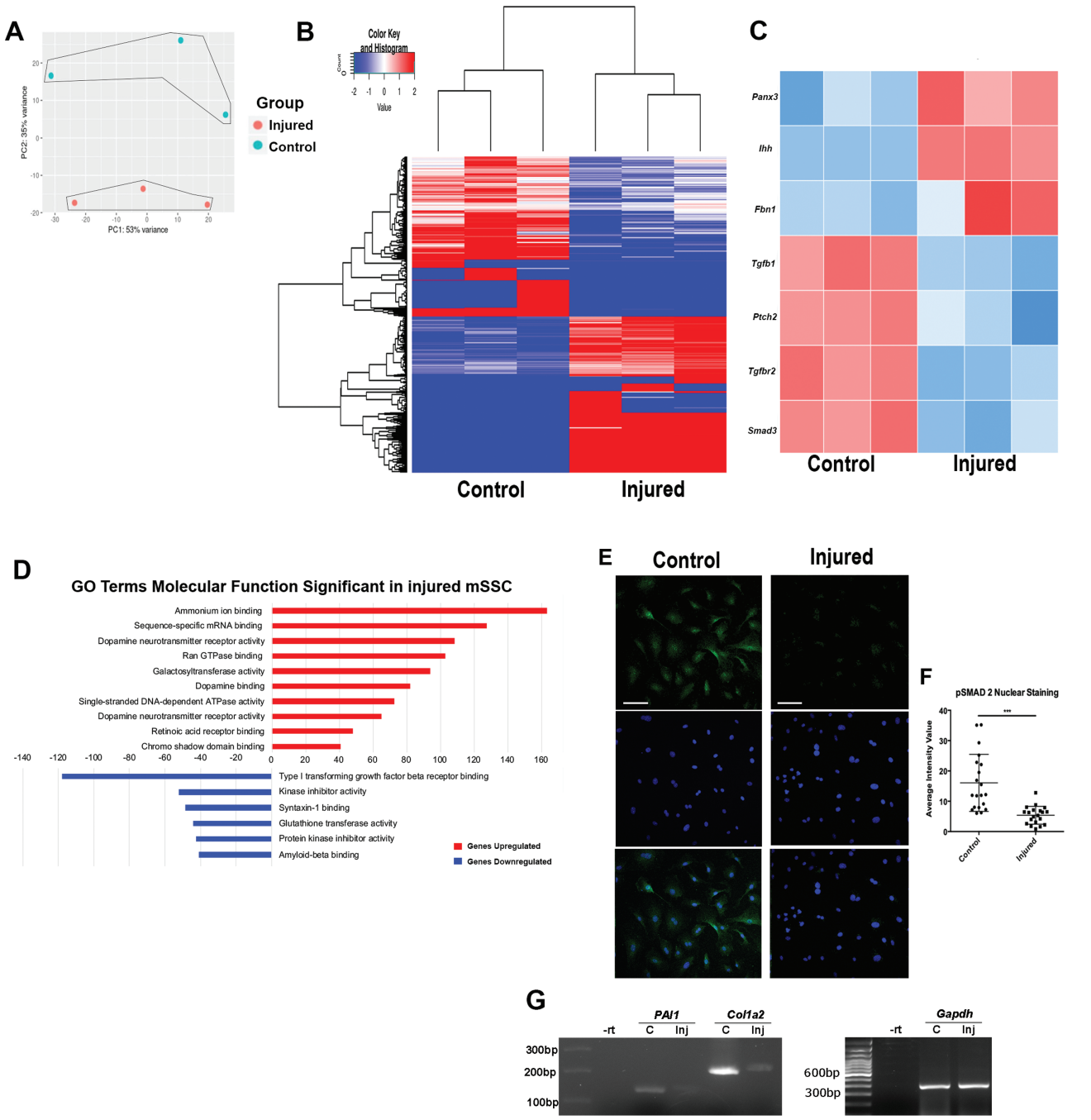

Figure 3. Transcriptomic profile demonstrates downregulation of TGFβ signaling components in mSSCs isolated from injured TBI. (**A**) Principal component analysis plot shows clustering of mSSCs FACs sorted specimens from injured and control tissues (n = 5 pooled, with 3 replicates) at post-injury day 7. (**B**) Heatmap of bulk RNA-seq data showing differential peaks (log2(normalized reads in peaks)) of injured mSSCs and control mSSC cohorts gene expression from post-injury day 7. Gene enrichment is noted in color key and histogram at the upper left. (**C**) Heatmap of selected genes of interest from overall heatmap differential peaks with significant upregulation of the Indian hedgehog pathway and downregulation of the TGFβ pathway. (**D**) GO terms enriched for genes upregulated (red) and downregulated (blue) in injured versus control mSSCs at post-injury day 7, identified by bulk RNA-seq. Select GO terms with significant P-values (Fischer exact test) are shown. (**E**) Injured mSSCs showed decreased image intensity of the nuclear localization of pSMAD2 (green) compared to control mSSCs ($P < .001$). Immunofluorescence of pSMAD2 (top column), DAPI staining (middle column), and merged images are shown. Original magnification: 20×. The image is representative of 3 experiments. (**F**) Significant decrease in quantified mSSC pSMAD2 immunofluorescence image intensity after injury which was performed with ImageJ and photoshop software. **G**, RT-PCR assay confirmed *Col1a* and *Pal1* were downregulated in injured mSSCs compared to sham control (n = 15 pooled mice).

lineage cells.[58] TGF-β1 may initially improve an injured TBI's overall strength due to scarring compared to untreated injuries, but it does not restore the pre-injury TBI morphology and overall biomechanical properties.[59] As a comparison, fetal wound healing, where no scars are seen, is characterized by low expression of TGF-β1, while adult wound healing is characterized by high levels of TGF-β1 and typically excessive scar formation.[60-64] The administration TGF-β1 to mSSCs in culture does not result in the expansion of mSSCs, but rather altered the morphology

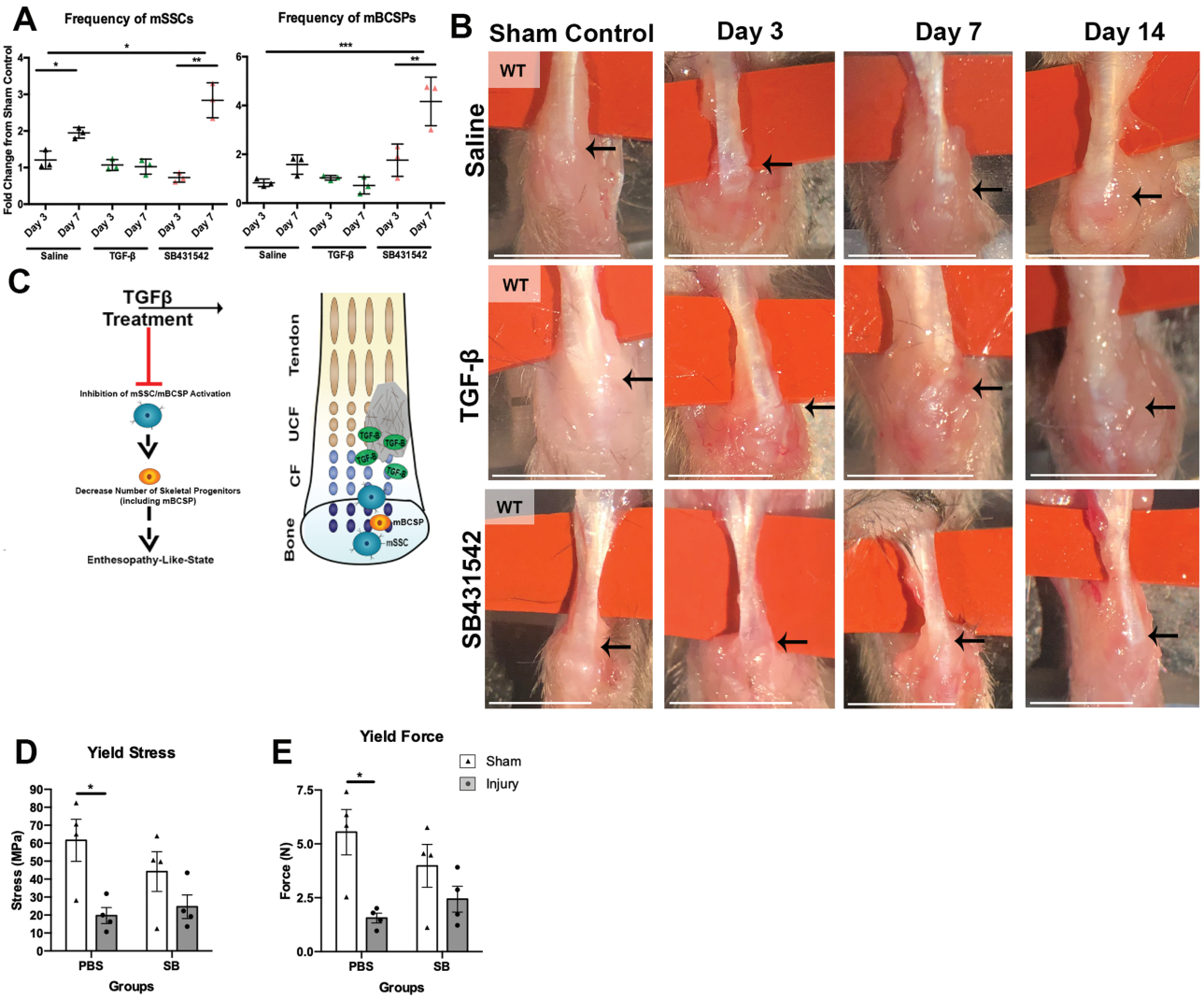

Figure 4. Treatment with exogenous TGFβ negatively impacts the activation of mSSCs in the Achilles tendon leading to an enthesopathy-like phenotype. (**A**) Quantification of the cellular frequency of FACS isolated mSSC demonstrated a significantly reduced response of mSSC and mBCSP post-injury after administration of exogenous TGFβ-1 compared to saline administration, and a significantly increased response with SB431542 treatment (n = 2 pooled, with 3 replicates). (**B**) Representative gross images of wild-type mice (3 panels) at post-injury days 3, 7, and 14 treated with saline control (top panel), TGFβ (second panel), and SB431542 (third panel). TBI injury identified with an arrow, Scale bars, 5 mm. (**C**) Schematic of proposed mSSC response during TBI healing in the setting of exogenous TGFβ. Following injury and administration of TGFβ1, mSSC response is inhibited, which also reduces the number of downstream progenitors present at the injury site. (**D**) Overall yield force 7 days post-injury was significantly reduced in injured Achilles TBIs treated with PBS. This significant reduction was mitigated in injured Achilles TBI treated with SB43154 (n = 4 per group). (**E**) Seven days post-injury there was a significant difference seen the yield stress seen in TBIs treated with PBS; with the treatment of SB43154 the difference was no longer significant. Data and error bars shown as mean ± SD.

of colony[13]; while administration of exogenous BMP-2 resulted in the rapid expansion of mSSCs[13] and has also been shown to have a positive impact on tendon healing,[65] suggesting the need for future investigation. Interestingly, TGF-β1 has been shown to possibly facilitate tenogenic differentiation of bone marrow-derived mesenchymal stem cells,[66,67] suggesting that TGF-β1 may have different effects on mSSCs versus bone marrow-derived mesenchymal stem cells.

Pathologically high concentrations of active TGFβ can impact the recruitment and proliferation of mesenchymal stem cells[68] as well as a subset of bone marrow precursor-cells, defined by *Nestin* positivity, contributing to the pathogenesis of enthesopathy.[12] This Nestin+ lineage, with known endothelial and mesenchymal lineage-cell specification, is unlikely to promote TBI-regeneration. Given that endogenous activation of TGFβ signaling increases Nestin+ cells in tendons, we sought to investigate whether administration of exogenous TGFβ would impact the prevalence of mSSCs post-injury. We observed a reduced mSSC response with post-injury exogenous TGFβ treatment in wild-type. Furthermore, the mSSC response was augmented beyond the control in mice treated with SB431542, a TGFβ inhibitor. These data indicate that, contrary to previous reports on Nestin+ lineage cells, after TBI injury mSSCs may orchestrate downregulation of TGFβ signaling to permit their expansion and eventual contribution to TBI regeneration. This is demonstrated by the fact that mSCCs expand after acute injury and downregulate TGFβ signaling, while exogenous administration of TGFβ attenuates the mSSC response/activation after TBI injury.

Increased TGFβ-1 is associated not only with enthesopathy and poor TBI healing but also with pathologic bone formation

states, including heterotopic ossification and osteoarthritis.[69,70] In contrast, inhibiting TGFβ signaling attenuates the progression of such disease processes and promotes the endogenous regenerative potential of the mammalian calvarium after injury.[71] This elevated signaling alters enthesis organized morphology.[12] mSSCs are activated in response to a TBI-injury and attempt to encourage TBI-regeneration via downregulation of TGFβ signaling within the mSSC niche.

It is important to note that our findings are specific to acute transection of a normal tendon that was not immobilized. Future research is required to evaluate the role of mSSCs in the setting of degenerative tendon/TBI injury that typically occurs in humans. Further, given that we used only Black 6 and rainbow mice strains in the study, there may be species- or strain-specific differences that limit the scope of the findings. Regarding our statistical methods, we ran the Shapiro–Wilk test on our data and found that for the immunofluorescence where there are 20 replicates, it met the assumptions for parametric testing via the Shapiro–Wilk's test, however, the sample sizes for our other results were too small (<5) to test for normality. Additionally, the study only covers the early phase of TBI repair as it uses early time points, and as a result future studies with longer time points are needed to investigate the long-term role of mSSCs in TBI healing and tissue remodeling.

Conclusion

Collectively, our results frame a conceptual advance in the understanding of tendon-to-bone regeneration by demonstrating, the involvement of a skeletal stem cell population in tendon-to-bone healing. Furthermore, these findings suggest that mSSCs play a role in repair and regeneration through the downregulation of TGFβ signaling. These mSSC and TGFβ pathway interactions may represent potential targets for medical interventions aimed at mitigating the painful and persistent enthesopathy that develops after partial enthesis injury.

Acknowledgments

The authors acknowledge Vida Shokoohi and the Stanford Functional Genomics Facility for assistance with gene expression experiments (supported by NIH S10OD018220), Julika Huber for histological assistance, and William McBride for manuscript preparation advice. The Beckman Cell Sciences Imaging Facility (supported by NIH 1S10OD01058001A1), the Stanford Stem Cell FACS Core, and the Stanford Nano Shared Facilities (supported by National Science Foundation ECCS-1542152).

Funding

This work was supported by the following awards: American College of Surgeons Resident Research Scholarships (ALT), the Stanford Transplant and Tissue Engineering Center of Excellence Fund (ALT), the Gunn/Olivier Fund (MTL), the California Institute for Regenerative Medicine (MTL), the Hagey Laboratory for Pediatric Regenerative Medicine (MTL), Stinehart/Reed Foundation (MTL), NIH 1R01DE027323 (MTL), and NIH 1RO1DE02730 (MTL).

Conflicts of Interest

The authors declared no potential conflicts of interest.

Author Contributions

A.L.T.: conception and design, financial support, administrative support, collection of data, data analysis, and interpretation, manuscript writing. M.D.: collection of data, data analysis, and manuscript writing. D.F.: study design, data collection, analysis and interpretation, and final approval of the manuscript. A.S., S.M., K.C.: data collection, analysis and interpretation, and final approval of the manuscript. E.F.: data collection and final approval of the manuscript. M.L.: data collection, analysis, and final approval of the manuscript. R.E.J., P.F.: study design, data interpretation, and manuscript writing. I.B.: data interpretation and manuscript writing. A.B.: data analysis, final approval of the manuscript. M.J.: data analysis and interpretation, manuscript writing. G.G.: data interpretation and final approval of the manuscript. C.C.: study design, data interpretation, and writing of the manuscript. N.Q.: conception and design, collection of data, data analysis and interpretation, and manuscript writing. M.T.L.: conception and design, financial support, administrative support, data interpretation, and manuscript writing.

Data Availability

Data to support the conclusions drawn in this manuscript can be found in the primary figures. All RNA-seq data can be accessed from the Gene Expression Omnibus (GEO, accession number GSE167080, https://www.ncbi.nlm.nih.gov/geo/query/acc.cgi?acc=GSE167080).

Supplementary Material

Supplementary material is available at Stem *Cells Translational Medicine* online.

References

1. Rossetti L, Kuntz LA, Kunold E, et al. The microstructure and micromechanics of the tendon-bone insertion. *Nat Mater*. 2017;16(6):664-670.
2. Thomopoulos S, Genin GM, Galatz LM. The development and morphogenesis of the tendon-to-bone insertion what development can teach us about healing. *J Musculoskelet Neuronal Interact*. 2010;10(1):35-45.
3. Thomopoulos S, Williams GR, Gimbel JA, et al. Variation of biomechanical, structural, and compositional properties along the tendon to bone insertion site. *J Orthop Res*. 2003;21(3):413-419.
4. Thomopoulos S, Williams GR, Soslowsky LJ. Tendon to bone healing: differences in biomechanical, structural, and compositional properties due to a range of activity levels. *J Biomech Eng*. 2003;125(1):106-113.
5. Kult S, Olender T, Osterwalder M, et al. Bi-fated tendon-to-bone attachment cells are regulated by shared enhancers and KLF transcription factors. *Elife*. 2021;10:e55361.
6. Itoi E, Berglund LJ, Grabowski JJ, et al. Tensile properties of the supraspinatus tendon. *J Orthop Res*. 1995;13(4):578-584.
7. Matsuhashi T, Hooke AW, Zhao KD, et al. Tensile properties of a morphologically split supraspinatus tendon. *Clin Anat*. 2014;27(5):702-706.
8. Deymier AC, An Y, Boyle JJ, et al. Micro-mechanical properties of the tendon-to-bone attachment. *Acta Biomater*. 2017;56:25-35.
9. Sano H, Saijo Y, Kokubun S. Non-mineralized fibrocartilage shows the lowest elastic modulus in the rabbit supraspinatus tendon insertion: measurement with scanning acoustic microscopy. *J Shoulder Elbow Surg*. 2006;15(6):743-749.
10. Wang D, Tan H, Lebaschi AH, et al. Kartogenin enhances collagen organization and mechanical strength of the repaired enthesis in

a murine model of rotator cuff repair. *Arthroscopy*. 2018;34(9):2579-2587.
11. Voleti PB, Buckley MR, Soslowsky LJ. Tendon healing: repair and regeneration. *Annu Rev Biomed Eng*. 2012;14:47-71.
12. Wang X, Xie L, Crane J, et al. Aberrant TGF-beta activation in bone tendon insertion induces enthesopathy-like disease. *J Clin Investig*. 2018;128(2):846-860.
13. Chan CK, Seo EY, Chen JY, et al. Identification and specification of the mouse skeletal stem cell. *Cell*. 2015;160(1-2):285-298.
14. Gulati GS, Murphy MP, Marecic O, et al. Isolation and functional assessment of mouse skeletal stem cell lineage. *Nat Protocols*. 2018;13(6):1294-1309.
15. Tevlin R, Seo EY, Marecic O, et al. Pharmacological rescue of diabetic skeletal stem cell niches. *Sci Transl Med*. 2017;9(372):eaag2809.
16. Ransom RC, Carter AC, Salhotra A, et al. Mechanoresponsive stem cells acquire neural crest fate in jaw regeneration. *Nature*. 2018;563(7732):514-521.
17. Jones RE, Salhotra A, Robertson KS, et al. Skeletal stem cell-schwann cell circuitry in mandibular repair. *Cell Rep*. 2019;28(2757-2766):2757-2766.e2755.
18. Menon S, Salhotra A, Shailendra S, et al. Skeletal stem and progenitor cells maintain cranial suture patency and prevent craniosynostosis. *Nat Commun*. 2021;12:4640.
19. Chan CKF, Gulati GS, Sinha R, et al. Identification of the human skeletal stem cell. *Cell*. 2018;175(1):43-56.e21.
20. Murphy MP, Koepke LS, Lopez MT, et al. Articular cartilage regeneration by activated skeletal stem cells. *Nat Med*. 2020;26(10):1583-1592.
21. Marecic O, Tevlin R, McArdle A, et al. Identification and characterization of an injury-induced skeletal progenitor. *Proc Natl Acad Sci USA*. 2015;112(32):9920-9925.
22. Chan CK, Lindau P, Jiang W, et al. Clonal precursor of bone, cartilage, and hematopoietic niche stromal cells. *Proc Natl Acad Sci USA*. 2013;110(31):12643-12648.
23. Ransom RC, Foster DS, Salhotra A, et al. Genetic dissection of clonal lineage relationships with hydroxytamoxifen liposomes. *Nat Commun*. 2018;9(1):2971.
24. Beason DP, Kuntz AF, Hsu JE, et al. Development and evaluation of multiple tendon injury models in the mouse. *J Biomech*. 2012;45(8):1550-1553.
25. Robinson PS, Huang TF, Kazam E, et al. Influence of decorin and biglycan on mechanical properties of multiple tendons in knockout mice. *J Biomech Eng*. 2005;127(1):181-185.
26. Kuleshov MV, Jones MR, Rouillard AD, et al. Enrichr: a comprehensive gene set enrichment analysis web server 2016 update. *Nucleic Acids Res*. 2016;44(W1):W90-W97.
27. Chen EY, Tan CM, Kou Y, et al. Enrichr: interactive and collaborative HTML5 gene list enrichment analysis tool. *BMC Bioinf*. 2013;14:128.
28. Quarto N, Wan DC, Kwan MD, et al. Origin matters: differences in embryonic tissue origin and Wnt signaling determine the osteogenic potential and healing capacity of frontal and parietal calvarial bones. *J Bone Miner Res*. 2010;25(7):1680-1694.
29. Rinkevich Y, Montoro DT, Contreras-Trujillo H, et al. In vivo clonal analysis reveals lineage-restricted progenitor characteristics in mammalian kidney development, maintenance and regeneration. *Cell Rep*. 2014;7(4):1270-1283.
30. Ueno H, Weissman IL. Clonal analysis of mouse development reveals a polyclonal origin for yolk sac blood islands. *Dev Cell*. 2006;11(4):519-533.
31. Hojo H, Ohba S, He X, et al. Sp7/Osterix is restricted to bone-forming vertebrates where it acts as a Dlx co-factor in osteoblast specification. *Dev Cell*. 2016;37(3):238-253.
32. Sinha KM, Zhou X. Genetic and molecular control of Osterix in skeletal formation. *J Cell Biochem*. 2013;114(5):975-984.
33. Nakashima K, Zhou X, Kunkel G, et al. The novel zinc finger-containing transcription factor osterix is required for osteoblast differentiation and bone formation. *Cell*. 2002;108(1):17-29.
34. Ishikawa M, Yamada Y. The role of pannexin 3 in bone biology. *J Dent Res*. 2017;96(4):372-379.
35. Iwamoto T, Nakamura T, Doyle A, et al. Pannexin 3 regulates intracellular ATP/cAMP levels and promotes chondrocyte differentiation. *J Biol Chem*. 2010;285(24):18948-18958.
36. Hung CT, Allen FD, Mansfield KD, et al. Extracellular ATP modulates $[Ca^{2+}]i$ in retinoic acid-treated embryonic chondrocytes. *Am J Physiol*. 1997;272(5):C1611-C1617.
37. Zong JC, Mosca MJ, Degen RM, et al. Involvement of Indian hedgehog signaling in mesenchymal stem cell-augmented rotator cuff tendon repair in an athymic rat model. *J Shoulder Elbow Surg*. 2017;26(4):580-588.
38. Liu CF, Breidenbach A, Aschbacher-Smith L, et al. A role for hedgehog signaling in the differentiation of the insertion site of the patellar tendon in the mouse. *PLoS One*. 2013;8(6):e65411.
39. Schwartz AG, Long F, Thomopoulos S. Enthesis fibrocartilage cells originate from a population of Hedgehog-responsive cells modulated by the loading environment. *Development (Cambridge, England)*. 2015;142(1):196-206.
40. Benjamin M, Toumi H, Ralphs JR, et al. Where tendons and ligaments meet bone: attachment sites ("entheses") in relation to exercise and/or mechanical load. *J Anat*. 2006;208(4):471-490.
41. Nistala H, Lee-Arteaga S, Smaldone S, et al. Fibrillin-1 and -2 differentially modulate endogenous TGF-β and BMP bioavailability during bone formation. *J Cell Biol*. 2010;190(6):1107-1121.
42. Roberts RR, Bobzin L, Teng CS, et al. FGF signaling patterns cell fate at the interface between tendon and bone. *Development (Cambridge, England)*. 2019;146(15):dev170241.
43. Blitz E, Sharir A, Akiyama H, et al. Tendon-bone attachment unit is formed modularly by a distinct pool of Scx- and Sox9-positive progenitors. *Development (Cambridge, England)*. 2013;140:2680-2690.
44. Blitz E, Viukov S, Sharir A, et al. Bone ridge patterning during musculoskeletal assembly is mediated through SCX regulation of Bmp4 at the tendon-skeleton junction. *Dev Cell*. 2009;17(6):861-873.
45. Derynck R, Zhang YE. Smad-dependent and Smad-independent pathways in TGF-β family signalling. *Nature*. 2003;425(6958):577-584.
46. Ignotz RA, Massagué J. Transforming growth factor-beta stimulates the expression of fibronectin and collagen and their incorporation into the extracellular matrix. *J Biol Chem*. 1986;261(9):4337-4345.
47. Keeton MR, Curriden SA, van Zonneveld AJ, et al. Identification of regulatory sequences in the type 1 plasminogen activator inhibitor gene responsive to transforming growth factor beta. *J Biol Chem*. 1991;266(34):23048-23052.
48. Vogel KG, Koob TJ. Structural specialization in tendons under compression. *Int Rev Cytol*. 1989;115:267-293.
49. Robbins JR, Evanko SP, Vogel KG. Mechanical loading and TGF-beta regulate proteoglycan synthesis in tendon. *Arch Biochem Biophys*. 1997;342(2):203-211.
50. Davies MR, Liu X, Lee L, et al. TGF-β small molecule inhibitor SB431542 reduces rotator cuff muscle fibrosis and fatty infiltration by promoting fibro/adipogenic progenitor apoptosis. *PLoS One*. 2016;11(5): e0155486.
51. Inman GJ, Nicolás FJ, Callahan JF, et al. SB-431542 is a potent and specific inhibitor of transforming growth factor-beta superfamily type I activin receptor-like kinase (ALK) receptors ALK4, ALK5, and ALK7. *Mol Pharmacol*. 2002;62(1):65-74.
52. Pryce BA, Watson SS, Murchison ND, et al. Recruitment and maintenance of tendon progenitors by TGFbeta signaling are essential for tendon formation. *Development (Cambridge, England)*. 2009;136(8):1351-1361.
53. Kaji DA, Howell KL, Balic Z, et al. Tgfβ signaling is required for tenocyte recruitment and functional neonatal tendon regeneration. *eLife* 2020;9:e51779.
54. Yang T, Grafe I, Bae Y, et al. E-selectin ligand 1 regulates bone remodeling by limiting bioactive TGF-beta in the bone microenvironment. *Proc Natl Acad Sci USA*. 2013;110(18):7336-7341.
55. Tang Y, Wu X, Lei W, et al. TGF-beta1-induced migration of bone mesenchymal stem cells couples bone resorption with formation. *Nat Med*. 2009;15(7):757-765.

56. Wang Y, Zhou Z, Liu Y, et al. Inhibition of Smad3 promotes the healing of rotator cuff injury in a rat model. *J Orthop Res*. 2021;39(1):204-218.
57. Galatz LM, Sandell LJ, Rothermich SY, et al. Characteristics of the rat supraspinatus tendon during tendon-to-bone healing after acute injury. *J Orthop Res*. 2006;24(3):541-550.
58. Arimura H, Shukunami C, Tokunaga T, et al. TGF-β1 Improves biomechanical strength by extracellular matrix accumulation without increasing the number of tenogenic lineage cells in a rat rotator cuff repair model. *Am J Sports Med*. 2017;45(10):2394-2404.
59. Jensen PT, Lambertsen KL, Frich LH. Assembly, maturation, and degradation of the supraspinatus enthesis. *J Shoulder Elbow Surg*. 2018;27(4):739-750.
60. Wang R, Ghahary A, Shen Q, et al. Hypertrophic scar tissues and fibroblasts produce more transforming growth factor-beta1 mRNA and protein than normal skin and cells. *Wound Repair Regen*. 2000;8(2):128-137.
61. Manning CN, Kim HM, Sakiyama-Elbert S, et al. Sustained delivery of transforming growth factor beta three enhances tendon-to-bone healing in a rat model. *J Orthop Res*. 2011;29(7):1099-1105.
62. Beredjiklian PK, Favata M, Cartmell JS, et al. Regenerative versus reparative healing in tendon: a study of biomechanical and histological properties in fetal sheep. *Ann Biomed Eng*. 2003;31(10):1143-1152.
63. Soo C, Beanes SR, Hu FY, et al. Ontogenetic transition in fetal wound transforming growth factor-beta regulation correlates with collagen organization. *Am J Pathol*. 2003;163(6):2459-2476.
64. Shah M, Foreman DM, Ferguson MW. Neutralisation of TGF-beta 1 and TGF-beta 2 or exogenous addition of TGF-beta 3 to cutaneous rat wounds reduces scarring. *J Cell Sci*. 1995;108(3):985-1002.
65. Pelled G, Snedeker JG, Ben-Arav A, et al. Smad8/BMP2-engineered mesenchymal stem cells induce accelerated recovery of the biomechanical properties of the Achilles tendon. *J Orthop Res*. 2012;30(12):1932-1939.
66. Yin Z, Guo J, Wu TY, et al. Stepwise differentiation of mesenchymal stem cells augments tendon-like tissue formation and defect repair in vivo. *Stem Cells Transl Med*. 2016;5(8):1106-1116.
67. Xu T, Xu M, Bai J, et al. Tenocyte-derived exosomes induce the tenogenic differentiation of mesenchymal stem cells through TGF-β. *Cytotechnology*. 2019;71(1):57-65.
68. Crane JL, Cao X. Bone marrow mesenchymal stem cells and TGF-β signaling in bone remodeling. *J Clin Invest*. 2014;124(2):466-472.
69. Zhen G, Wen C, Jia X, et al. Inhibition of TGF-beta signaling in mesenchymal stem cells of subchondral bone attenuates osteoarthritis. *Nat Med*. 2013;19(6):704-712.
70. Wang X, Li F, Xie L, et al. Inhibition of overactive TGF-beta attenuates progression of heterotopic ossification in mice. *Nat Commun*. 2018;9(1):551.
71. Senarath-Yapa K, Li S, Walmsley GG, et al. Small molecule inhibition of transforming growth factor beta signaling enables the endogenous regenerative potential of the mammalian calvarium. *Tissue Eng Part A*. 2016;22(9-10):707-720.